Design, Simulation and Comparison of two $15mm \times 15mm$ UWB Antennas with Modified Ground Patch for High Data-rate Wireless Electrophysiological Recording Application

Adnan Basir Patwary, and Ifana Mahbub
Department of Electrical Engineering, University of North Texas, Denton, TX, USA

***Abstract*—For the diagnosis and treatment of various chronic neurological diseases such as Epilepsy, Seizure and, chronic pain, a long-term electrophysiological recording and stimulation are required for the patients. This type of study can be done through implantable neuromodulation devices. One of the key challenges in designing such implantable medical devices is the size restriction. Even the antennas transmitting the recorded signals must be small, miniaturized, and light-weight in order for the small animals used in the clinical studies to carry it easily. In this paper, two $15mm \times 15mm$ antennas are designed which have ultra-wide bandwidths making them suitable for the high data rate electrophysiological recording applications. The proposed antennas are bidirectional and along with being small in size make them suitable to be added to the headstage based electrophysiological recording devices. Both antennas have a similar radiating patches with each ground patch modified by creating two different slots. A comparison of the proposed antenna has also been presented in the paper where both the antennas operating between 4.7 GHz and 8.3 GHz and having average gains above 4.35 dBi. Though the proposed antennas are 40% smaller in size, they have 6% higher gain compared to the state of the art.**

***Index Terms*—Neural signal acquisition, Microstrip Antenna, Ultra Wideband Antenna.**

I. Introduction

Implantable medical devices have become very popular due to the high demand for advanced medical treatment and long-term monitoring of chronic neural diseases such as Epilepsy, Seizure and, chronic pain. Deep brain stimulation and neuromodulation are an essential part of these treatments [1]. In developing such implantable medical devices, a model which uses a headset-based wirelessly powered brain neuromodulation and neural stimulation system to continuously monitor neural activities of freely moving animals is proposed in [2]–[4]. In order to monitor the neural activities, continuous wireless telemetry needs to be established between the implanted biomedical sensor and the monitoring devices. Implantable biomedical sensors and devices developed to monitor the freely-moving animals are subjected to size and energy constraints. Meanwhile, wireless communication using UWB band is highly energy efficient because of the narrow pulsed based communication and the radio can be aggressively duty-cycled. Therefore, for the wireless telemetry, a duty-cycled IR-UWB transmitter designed using 180 nm CMOS process is proposed in our prior work that achieves a high energy efficiency and high data rate [5]. The transmitter works in the frequency range of 4 GHz - 7 GHz and the bandwidth can be reconfigured from 500 MHz to 950 MHz, making it suitable for high data rate wireless data telemetry. A small-sized UWB antenna operating in the 3.1 GHz to 10 GHz frequency range is required to transmit the electrophysiological signal at the receiving end which has the monitoring device, a PC with the software for further signal processing such as spike sorting and classification to be monitored and recorded. The electrophysiological signals are transmitted from multiple channels (> 128 channels) where each channel is sampled at 40 kbps rate with an Analog-to-digital resolution of 16 bits making the total data rate close to 100 Mbps which requires ultra-wideband transceivers and antennas. Fig. 1 depicts the wireless electrophysiological recording and monitoring system for free-moving animals.

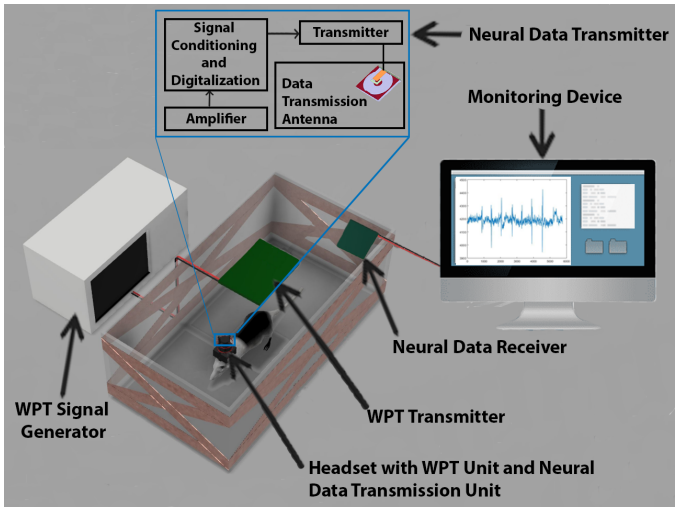

Fig. 1: Wireless Electrophysiological Recording and Monitoring System

Conventional UWB antennas that operate within the required frequency range (4GHz - 7GHz) are larger in size ranging from $22mm \times 22mm$ to $55mm \times 55mm$. [6], [7] and [8] propose antenna models that operate within 2.3GHz - 11GHz but the size of the antenna are $25mm \times 25mm$, $22mm \times 16mm$ and $49mm \times 55mm$ respectively, which are much larger in size for the headstage based recording system presented in our earlier work [4]. The antennas also have lower gains (less than

978-0-7381-1299-2/21/$31.00 ©2021 IEEE

4.11 dBi). Moreover, the antennas are unidirectional antennas. This paper proposes the design and comparison of two novel antenna architectures that have $15mm \times 15mm$ dimension with a similar radiating patches which are 50Ω transmission line with a parasitic patch. The small size requires the antennas to operate at a higher frequency range and the ground plane is modified by creating two different slots for the two different antennas. Both the antennas operate in the frequency range covered by the transmitter mentioned in our prior work [5] with gains higher than 4.33 dBi.

The main contributions of this paper are the development of antenna structures being small in size ($15mm \times 15mm$) with a 50Ω transmission line and an inverted L-shaped parasite as the radiating patch and slotted ground plane. The novelty of this work lies in the modeling technique for the two different antenna architectures for the different shaped slots with the added stubs for improving the bandwidth. This work also presents a detailed comparative analysis between the two proposed antennas. The paper is organized as follows: section II discusses the design and modeling of the antennas; section III presents the simulation results, followed by a concluding remarks presented in section IV.

II. Antenna Architecture and Modeling

The architecture of the proposed antennas is illustrated in Fig. 2 and Fig. 4 and their design parameters are also given in Table I and Table II. Both of the proposed antennas are designed on a $15mm \times 15mm$ FR4 substrate with a dielectric constant, $\epsilon_r = 4.4$, and a height of 1.57 mm. Copper (Cu) with a height of 0.033mm has been used as the conductor for the radiating patch and the ground patch. The design steps of the proposed antennas are shown in Fig. 3 and Fig. 5. The first two steps are similar for both of the antennas, as they both have a similar radiating patch. The main difference in their design structure is the modification of their ground patch.

A. Radiating Patch Design

As both antennas have a similar radiating patch, in order to design the radiating patch, a simple $15mm \times 15mm$ patch antennas with full ground patches are designed in the first step. In the first step, the designed radiating patch is a 50Ω microstrip line with W_p width and L_p length. The signal is directly fed to the patch. Afterward in the second step, the radiating patch is further modified by adding an inverted L-shaped parasitic patch in close proximity of the microstrip line radiating patch to improve the overall bandwidth and return loss of the proposed antennas [9]. The inverted L-shaped parasitic patch has a dimension of 4.5mm on the longer side and 3.5mm on the shorter side with a width of 1 mm and is placed 0.5mm apart from the radiating patch.

B. Ground Patch Modification and Analysis

The two antennas consist of two different modified ground patches. The ground patches are modified by creating slots of different shapes. Fig. 2 represents the proposed antenna where the ground patch is modified by adding a square slot.

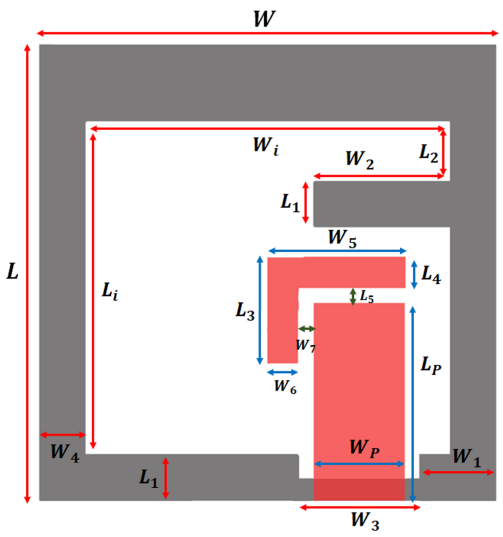

Fig. 2: 15mm Antenna with Square Slot in the ground patch.

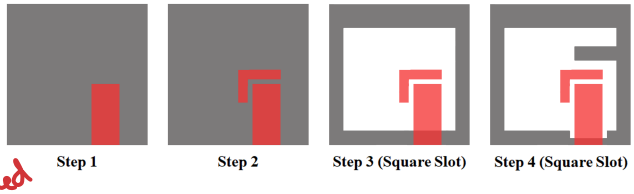

Fig. 3: Design procedure of the Square Slot Antenna.

The antenna design parameters for the 15 mm Square Slot Antenna are given in Table I. From the design procedure of the square Slot Antenna shown in Fig. 3 in the third step, after adding the radiating patch the ground patch is modified by adding a square slot of L_i length and W_i width. The value of L_i and W_i is determined using the following equation [6]:

$$W_i + L_i = 0.5\lambda_0 \sqrt{\left(\frac{1+\epsilon_r}{2\epsilon_r}\right)} \quad (1)$$

where λ_0 and ϵ_r represent the free-space wavelength at the lowest frequency of the bandwidth and the dielectric constant of the substrate, respectively. The square slot is added to create an ultra-wideband operating frequency at a lower frequency value. Finally, in the fourth step a horizontal stub of L_1 length and W_2 width is added in the ground patch above the radiating patch to create an extra resonant mode at a higher

TABLE I
15mm Square Slot Antenna Design Parameters

Parameter	Value (mm)	Parameter	Value (mm)
L	15	L_4	1
W	15	L_5	0.5
L_i	11	W_1	2.5
W_i	12	W_2	5
L_P	6.5	W_3	4
W_P	3	W_4	1.5
L_1	1.5	W_5	4.5
L_2	2	W_6	1
L_3	3.5	W_7	0.5

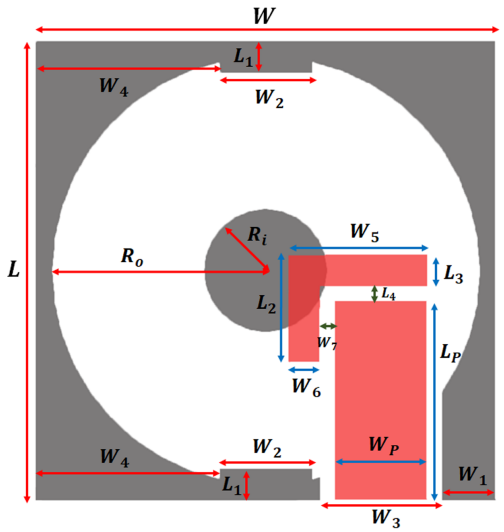

Fig. 4: 15mm Antenna with Ring Slot in the ground patch.

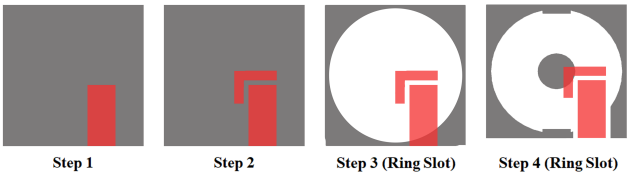

Fig. 5: Design procedure of the Ring Slot Antenna.

frequency and increase the bandwidth. The addition of UWB operating frequency at a lower frequency range and also 115% increase in bandwidth mentioned in design step 3 and step 4 respectively for the square slot antenna design process shown in Fig. 3 can be observed in Fig. 6 (a).

Fig. 4 depicts the proposed antenna where the ground patch is modified by adding a ring slot. The antenna design parameters for the 15 mm Ring slot antenna is shown in Table II. After adding the radiating patch, the ground patch is modified by adding a circle slot which can be observed in the third step of the design procedure of the ring slot antenna shown in Fig. 5. The radius of the circle slot is R_o and the value of R_o is determined using the following equation [10]:

$$R_o = \frac{1.84c}{2\pi f_c}\sqrt{\left(\frac{1+\epsilon_r}{2\epsilon_r}\right)} \tag{2}$$

where f_c represents the lowest resonating frequency, c represents the speed of light and ϵ_r represents the dielectric constant of the substrate, respectively. The circle slot is added so that the antenna resonates at a lower frequency value despite of being a small-sized antenna that normally resonates at higher frequency. This can be observed in Fig. 6 (b). In the fourth design step shown in Fig. 5, a circular parasitic patch of R_i is added in the ground slot to create an overall ring slot so that the antenna resonates at a lower frequency with a higher bandwidth. Along with that two small horizontal stubs of W_2 width are added on top and in the bottom of the ground patch to add an extra resonant mode in the higher frequency. As a result the antenna resonates within an ultra-wideband range which can also be observed in Fig. 6 (b).

TABLE II
15mm Ring Slot Antenna Design Parameters

Parameter	Value (mm)	Parameter	Value (mm)
L	15	L_4	0.5
W	15	W_1	1.75
R_o	7	W_2	3
R_i	2	W_3	4
L_P	6.5	W_4	6
W_P	3	W_5	4.5
L_1	1	W_6	1
L_2	3.5	W_7	0.5
L_3	1		

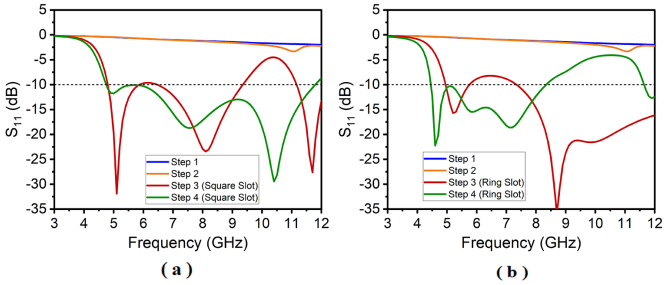

Fig. 6: Simulated change of S_{11} during design procedure for (a) Square Slot Antenna. (b) Ring Slot Antenna

III. Simulated Results

The antenna design and the simulations were performed using the Ansys High-frequency Structure Simulator (HFSS) software. The antennas were designed to operate as the transmitting antennas for the UWB Transmitter proposed in [5]. Fig. 7 represents the comparison of the S_{11} parameters of the proposed antennas. From the figure, it can be observed that the square slot antenna operates at a frequency range of 4.7 GHz to 11.6 GHz and the ring slot antenna operates in the range of 4.4 GHz to 8.3 GHz. The square slot antenna achieves a higher bandwidth (6.9 GHz) compared to the ring slot antenna (3.9 GHz) although the ring slot antenna can operate at a lower frequency.

Fig. 8 depicts the gain vs. frequency plots for the proposed antennas. From this figure, it can be observed that at the lower frequencies (4.4 GHz - 7.8 GHz) both the square slot and ring

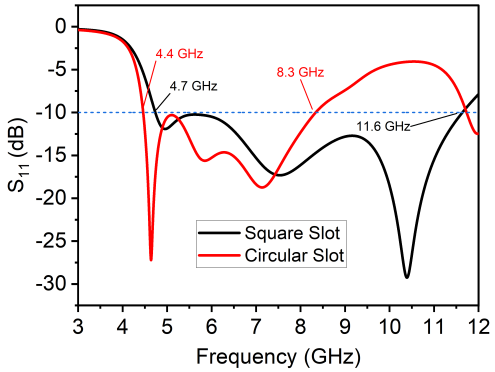

Fig. 7: Simulated S_{11} of the proposed antennas.

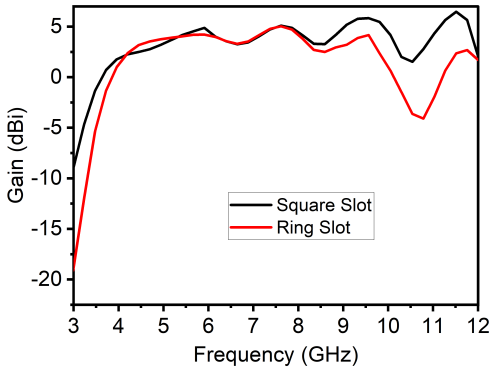

Fig. 8: Simulated Gain of the proposed Antennas.

slot antennas have almost similar gains ranging from 3 dBi to 4.9 dBi, where the highest gain is achieved at 7.6 GHz by both antennas. Nevertheless, at a higher frequency range (7.9 GHz - 11.6 GHz), the Square slot antenna achieves a higher gain with a maximum value of 6.8 dBi at 11.6 GHz.

Fig. 9 represents the 3D radiation pattern of the proposed antennas at 6.1 GHz. From the figure, it can be observed that both the antennas are bidirectional. The 2D radiation pattern of the proposed antennas at three different frequencies (4.7 GHz, 6.1 GHz and 7.6 GHz) can be observed from Fig. 10 where the radiation patterns are sliced at $\phi = 0°$ and $\phi = 90°$ and then plotted. At higher frequency (7.6 GHz), both the square slot and the ring slot antenna operate as a bidirectional antenna where the highest gain of 4.8 dB and 4.9 dB can be observed close to $\theta = 0°$ and $\theta = 180°$ respectively. The square slot antenna works as a bidirectional antenna at lower frequencies (4.7 GHz and 6.1 GHz). At lower frequencies (4.7 GHz and 6.1 GHz), the ring slot antenna also acts as a bidirectional antenna although, at 4.7 GHz it also operates in a third direction at $\theta = -90°$ and the gain is comparatively low at that direction (1.1 dB).

According to the discussion above, both of the proposed antennas in this paper are bidirectional and so they have two lobes 180° apart with a specific beam angle. Fig. 11 represents the plotted directive gain vs angle(θ) of the proposed antennas at three different frequency levels (4.7 GHz, 6.1 GHz and 7.6 GHz). The beam angles of the proposed antennas for the given

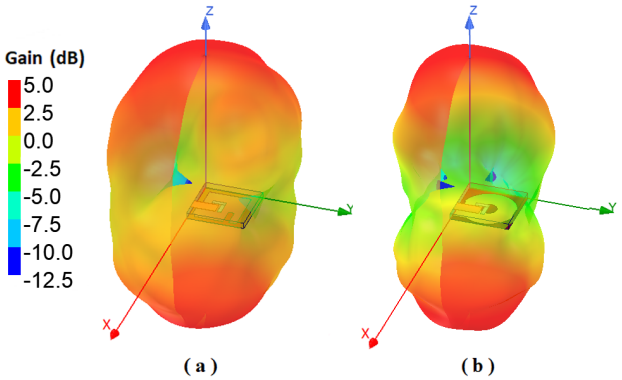

Fig. 9: 3D Radiation Pattern of (a) Square Slot Antenna. (b) Ring Slot Antenna.

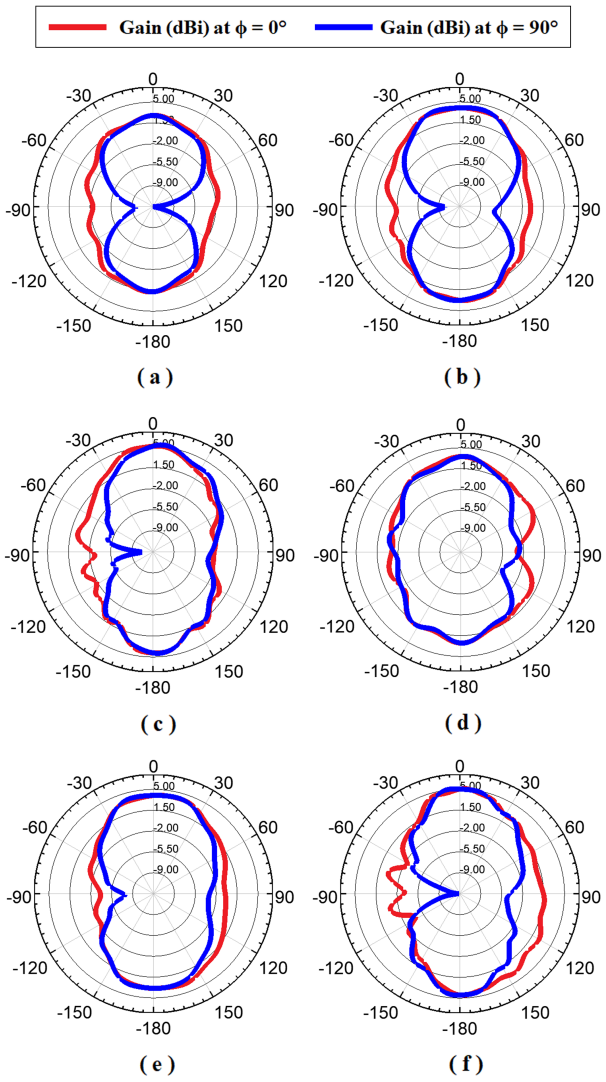

Fig. 10: Simulated Radiation Pattern at $\phi = 0°(Red)$ and $\phi = 90°(Blue)$ of (a) Square Slot Antenna at 4.7 GHz. (b) Square Slot Antenna at 6.1 GHz. (c) Square Slot Antenna at 7.6 GHz. (d) Ring Slot Antenna at 4.7 GHz. (e) Ring Slot Antenna at 6.1 GHz. (f) Ring Slot Antenna at 7.6 GHz

frequencies can be calculated from the data of the plots in Fig. 11. From the figure, it can be observed that at 4.7 GHz, the square slot Antenna has a beam angle of 105° and 100° and the ring slot antenna has a beam angle of 125° and 120° at $\phi = 0°$ and $\phi = 90°$, respectively. Furthermore, at 6.1 GHz, the square slot antenna has a beam angle of 135° and 100° and the ring slot antenna has a beam angle of 120° and 100° at $\phi = 0°$ and $\phi = 90°$ respectively. Finally, at 7.6 GHz, the square slot antenna has a beam angle of 140° and 110° and the ring slot antenna has a beam angle of 90° and 105° at $\phi = 0°$ and $\phi = 90°$, respectively.

Comparisons of the proposed antennas with other referred antennas are listed in Table III. The major advantage of the proposed antennas is that they are smaller in size compared to the previous works mentioned in Table III. The proposed

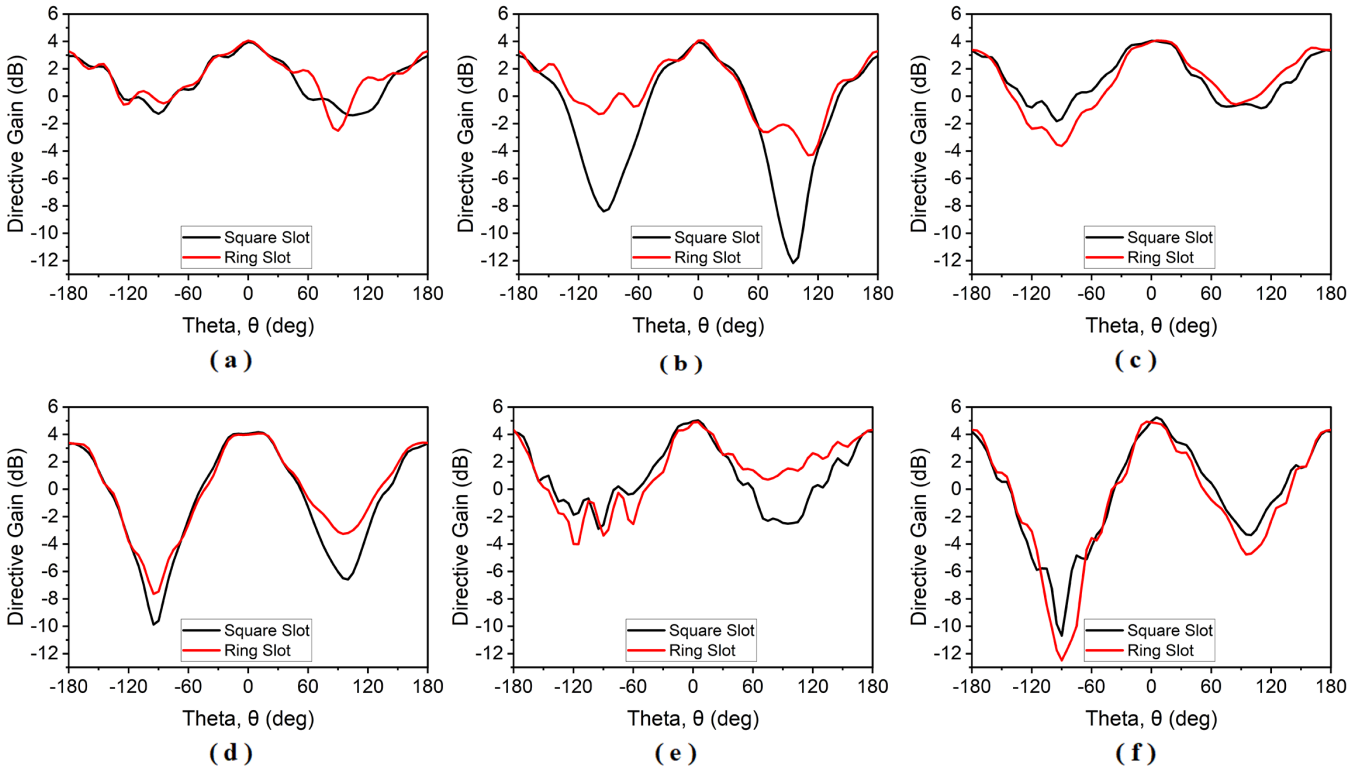

Fig. 11: Simulated Directive Gain vs Theta, θ for, (a) $\phi = 0°$ at 4.7 GHz. (b) $\phi = 90°$ at 4.7 GHz. (c) $\phi = 0°$ at 6.1 GHz. (d) $\phi = 90°$ at 6.1 GHz. (e) $\phi = 0°$ at 7.6 GHz. (f) $\phi = 90°$ at 7.6 GHz.

TABLE III
Comparison with other works

	[6]	**[9]**	**[7]**	**[8]**	**[11]**	**Proposed 15mm Square Slot**	**Proposed 15mm Ring Slot**
Size (mm × mm)	25×25	22.5×29.1	22×16	55×49	25×25	15×15	15×15
Frequency Range (GHz)	3.4-12.4	3.2-8	4.4-7.5	2.2-7.2	4.5-10.5	4.7-11.6	4.4-8.3
BW (GHz)	9	4.8	3.1	5	6	6.9	3.9
Gain (dBi)	4.3	3.47	5	4.11	3.5	4.6	4.39
Substrate	FR4	Rogers RO4003C	FR4	FR4	FR4	FR4	FR4
Substrate Height (mm)	1.7	0.813	1	1.5	1	1.57	1.57
Directionality	Uni-directional	Uni-directional	Uni-directional	Uni-directional	Uni-directional	Bi-directional	Bi-directional

antennas have 40% smaller size on average and 70% smaller than the largest antennas mentioned in the table making them suitable for the headstage model for electrophysiologial recording and monitoring. The proposed antennas have higher gains ($> 6\%$) and the proposed square slot antenna has an average of 52% higher bandwidth than most of the previous works mentioned in the table. The proposed antennas are also bidirectional compared to the other previous works which are unidirectional and thus it will reduce the number of receiving antennas.

IV. Conclusion

In this paper, two antennas have been proposed for neural signal transmission in wireless headstage based wireless neuromodulation devices. The small size ($15mm \times 15mm$) and their bidirectional radiation pattern makes them suitable for headstage based recording and monitoring devices. Both antennas have the same radiating patch consisting of 50Ω transmission line and a parasitic patch. The antennas are differentiated by modifying their ground patch by adding different shaped slots. The antenna with a modified square

slot as a ground patch has a total bandwidth of 6.9 GHz and an average gain of 4.6 dBi. The antenna with a modified ring slot as a ground patch has a total bandwidth of 3.9 GHz with an average gain of 4.39 dBi. The proposed antennas operate at the UWB frequency band suitable for the UWB transmitter. The future works include the fabrication and the extensive characterization of the fabricated antennas and a comparative analysis with the simulated model.

ACKNOWLEDGMENT

This work is based upon work supported by the National Science Foundation (NSF) under grant No. ECCS 1943990.

REFERENCES

[1] Y. Lin, C. Yeh, P. Huang, Z. Wang, H. Cheng, Y. Li, C. Chuang, P. Huang, K. Tang, H. Ma, Y. Chang, S. Yeh, and H. Chen, "A battery-less, implantable neuro-electronic interface for studying the mechanisms of deep brain stimulation in rat models," *IEEE Transactions on Biomedical Circuits and Systems*, vol. 10, no. 1, pp. 98–112, 2016.

[2] D. K. Biswas, B. Rangel, and I. Mahbub, "Design of a multi-layered on-chip wireless power transfer (wpt) system design for brain neuro-modulation applications," in *2020 IEEE Texas Symposium on Wireless and Microwave Circuits and Systems (WMCS)*, 2020, pp. 1–5.

[3] D. K. Biswas, J. H. A Martinez, I. Kaul, A. Kaul, and I. Mahbub, "A miniaturized highly efficient headstage based wireless power transfer (wpt) system for optogenetic stimulation of freely moving animals," in *2020 IEEE 14th Dallas Circuits and Systems Conference (DCAS)*, 2020, pp. 1–4.

[4] D. K. Biswas, J. H. A. Martinez, J. Daniels, A. Bendapudi, and I. Mahbub, "A novel 3-d printed headstage and homecage based wpt system for long-term behavior study of freely moving animals," in *2020 IEEE Radio and Wireless Symposium (RWS)*, 2020, pp. 268–271.

[5] D. K. Biswas and I. Mahbub, "A low-power duty-cycled impulse-radio ultrawideband (ir-uwb) transmitter with bandwidth and frequency reconfigurability scheme designed in 180 nm cmos process," in *2021 IEEE Radio and Wireless Symposium (RWS)*, 2021, pp. 49–52.

[6] P. L. Chi and M. H. Huang, "Compact circularly-polarized slot antenna with enhanced impedance and axial-ratio bandwidths," in *2019 IEEE Asia-Pacific Microwave Conference (APMC)*, 2019, pp. 446–448.

[7] K. O. Gyasi, G. Wen, D. Inserra, Y. Huang, J. Li, A. E. Ampoma, and H. Zhang, "A compact broadband cross-shaped circularly polarized planar monopole antenna with a ground plane extension," *IEEE Antennas and Wireless Propagation Letters*, vol. 17, no. 2, pp. 335–338, 2018.

[8] H. Tang, K. Wang, R. Wu, C. Yu, J. Zhang, and X. Wang, "A novel broadband circularly polarized monopole antenna based on c-shaped radiator," *IEEE Antennas and Wireless Propagation Letters*, vol. 16, pp. 964–967, 2017.

[9] U. Ullah, S. Koziel, and I. B. Mabrouk, "Rapid redesign and bandwidth/size tradeoffs for compact wideband circular polarization antennas using inverse surrogates and fast em-based parameter tuning," *IEEE Transactions on Antennas and Propagation*, vol. 68, no. 1, pp. 81–89, 2020.

[10] H. Zhang, Y. Jiao, L. Lu, and C. Zhang, "Broadband circularly polarized square-ring-loaded slot antenna with flat gains," *IEEE Antennas and Wireless Propagation Letters*, vol. 16, pp. 29–32, 2017.

[11] K. Ding, C. Gao, T. Yu, and D. Qu, "Broadband c-shaped circularly polarized monopole antenna," *IEEE Transactions on Antennas and Propagation*, vol. 63, no. 2, pp. 785–790, 2015.